ELSEVIER

Journal of Electroanalytical Chemistry 414 (1996) 209–220

JOURNAL OF ELECTROANALYTICAL CHEMISTRY

Impedance aspects of anion adsorption on gold single crystal electrodes

Tamás Pajkossy [1], Thomas Wandlowski *, Dieter M. Kolb

Department of Electrochemistry, University of Ulm, D-89069 Ulm, Germany

Received 14 February 1996; revised 27 March 1996

Abstract

In order to explore the origins of the capacitance dispersion observed for single crystal electrodes, voltammetric and impedance measurements on Au(111) and Au(100), in the absence and the presence of specifically adsorbed anions, mostly Br^-, have been carried out. Interfacial capacitances and rate coefficients characterizing the kinetics of adsorption have been evaluated from the impedance spectra. We present evidence that the double layer behaves as an ideal capacitance in the absence of specific adsorption. The approximation with a constant phase element yields an exponent larger than 0.99. The "capacitance dispersion" observed in the presence of specific adsorption is either assigned to a slow diffusion or adsorption process, or to transformations within the adlayer or the substrate surface.

Keywords: Anion adsorption; Impedance; Gold electrode

1. Introduction

Although solid electrodes have commonly been employed in studies aimed at describing mechanisms of electrode processes, major advances in deriving a microscopic picture of the bare and adsorbate-covered electrode surface, as well as in understanding the structure sensitivity of many interfacial reactions, have been achieved with the use of well-defined single crystal electrodes [1–4]. The combination of classical electrochemical techniques with in situ spectroscopic and structure-sensitive methods like electroreflectance [5], infrared spectroscopy [6], second harmonic generation [7], scanning probe microscopy [8,9] and surface X-ray scattering [10,11] provided fairly detailed atomic-scale information on electrochemical interfaces. Various phenomena and processes have been characterized employing this approach. Examples are the surface reconstruction of Au(*hkl*) in aqueous solutions [12], the underpotential deposition of copper on Au(*hkl*) [13] and lead on Ag(*hkl*) [14] or the adsorption of anions on low-index crystal faces of gold, silver and platinum [15–17]. Such structural data also allow light to be shed on some of the puzzling features of electrochemical measurements. One such issue is the frequency dependence of the double layer capacitance for ideally polarizable single crystal electrodes.

The frequency dependence of the interfacial capacitance (or briefly the capacitance dispersion) has been observed quite often, even in the absence of faradaic reactions. The effect can be due to various reasons: for example, the adsorption of organic as well as certain inorganic species onto the smooth and ideally polarizable mercury|electrolyte interface yields a typical adsorption impedance behaviour [18,19]. Other sources of capacitance dispersion can be surface roughness and heterogeneity [20]. Although surface heterogeneities should play a minor role for (perfect) single crystals, capacitance dispersion has been observed even then, e.g. by Hamelin and coworkers [3,4,21] in the frequency range $12\,Hz < f < 80\,Hz$ for low- and high-index gold single crystal electrodes in various electrolytes. These authors tentatively attributed their observations to the reconstruction of the substrate surface and to faradaic reactions associated with the incipient oxidation of gold. Capacitance dispersion was also reported for the adsorption of molecules on Au(*hkl*) [22,23]. Similar effects, though less pronounced, have also been observed on Ag(111) electrodes in the presence of F^-, SO_4^{2-} and CH_3COO^- ions [24,25].

* Corresponding author.

[1] Permanent address: KFKI Atomic Energy Research Institute, Budapest 114, POB 49, H-1525 Budapest, Hungary.

PII S0022-0728(96)04700-6

Capacitance dispersion may be related to either the solution side or the metal side of the electrochemical double layer. While the latter is rather complex and still only poorly understood, for the former there are fairly detailed theories available which describe the impedance characteristics due to slow diffusion and/or slow adsorption onto an electrode surface [18,26–28]. By employing these theories, the rate of adsorption can be determined, which may vary considerably for different systems. As an example, the adsorption rate of I^- on a Pt(111) surface was found to be immeasurably high [29], whereas that of CH_3COO^- on Ag(111) was rather slow [25], namely $k_{ad} = 6 \times 10^{-6}\,cm\,s^{-1}$.

The aim of this study is to explore the origins of the capacitance dispersion on single crystal electrodes. We have performed voltammetric and impedance measurements on two low-index planes of gold, Au(111) and Au(100), in the absence and the presence of specifically adsorbing anions, mostly bromide. From the impedance spectra, thermodynamic and kinetic parameters of the adsorption have been evaluated. Special emphasis was placed on the correlation of these parameters with the potential induced structural changes of the adlayer and the substrate surface.

2. Experimental

The Au(111) and Au(100) electrodes were single crystal cylinders with a diameter of 4 mm and a height of about 4 mm. A gold wire was attached to the rear for mounting purposes. Before each experiment the electrode was annealed in a Bunsen burner flame and, after a short period of cooling in air, quenched in "Milli-Q" water. Contact of the crystal with the electrolyte was established under potential control at $E = -0.60$ V (in neutral solutions) or $E = -0.20$ V (in acidic solutions) by employing the so-called "hanging meniscus technique". This procedure ensured the in situ stability of the substrate reconstruction, Au(111)-(23 × √3) or Au(100)-(hex), at the beginning of each experiment [10,12,30].

The solutions were prepared from "Milli-Q" water, $KClO_4$ (Fluka puriss, twice recrystallized), $HClO_4$ and NaBr (Merck, Suprapur). They were deaerated with 5N purity nitrogen before and during the measurements.

The electrochemical set-up consisted of a home-made potentiostat, a Stanford Research 830 digital lock-in amplifier, the analogue output voltages of which were digitized and transferred to a personal computer by a Digidata 1200 data acquisition board (Axon Instruments). The lock-in amplifier measured the a.c. voltage across an *RC* circuit connected in series with the counter electrode. This *RC* circuit, serving as a "reference impedance", had a frequency characteristic similar to that of the electrodes studied, and thus there was no need to adjust the amplification during frequency scans. The advantages of this a.c. current-to-voltage conversion are that calibrations are simple, noise levels are lower than that of the I/E converter of the potentiostat and, finally, high-frequency phase shifts of electronic origin can more easily be taken into account. The set-up was calibrated with dummy cells having impedance spectra rather similar to those of the systems studied. The maximum inaccuracy was about 1° of the phase angle and 1% of the magnitude at 10 kHz. The typical accuracy between 0.1 Hz and 1 kHz is about one order of magnitude better. However, the inhomogeneous current distribution in the hanging meniscus configuration and the rather high resistances between the cell compartments reduced the accuracy. The latter effect could be diminished effectively by employing auxiliary a.c. electrodes. These were platinum wires placed in the main compartment, connected to the counter and reference electrodes through capacitors of 1 and 20 μF respectively. The overall accuracy of electronics and cell was estimated to be about 1° and 1% at 1 kHz.

The measured impedance spectra are represented throughout this paper by calculating $C(\omega) = Y(\omega)/(i\omega) = 1/[Z(\omega) - Z(\omega \to \infty)]A_e i\omega$, where ω, $Z(\omega \to \infty) = R_s$ and A_e are the angular frequency, the solution resistance and the electrode area respectively. Because of its physical meaning, $C(\omega)$ is termed the "interfacial capacitance" and, being a complex quantity, can be plotted either in the Bode or in the complex representation (the latter is analogous to the Cole–Cole plot used in the context of dielectrics). In the same vein, the capacitance–voltage curve consists of two parts: the ReC–E plot is the "classical" C–E curve, whereas the ImC–E curve characterizes the "loss" rather than the charge-storing behaviour.

The equivalent circuit parameters were calculated by fitting the impedance function to the measured spectra by a non-linear least-squares program, which minimizes the sum of the $[(\mathrm{Re}Z - \mathrm{Re}Z_{calc})^2 + (\mathrm{Im}Z - \mathrm{Im}Z_{calc})^2]/\mathrm{Abs}Z^2$ terms for all frequencies measured. ReZ, ImZ and Abs$Z$ represent the real and imaginary components and the absolute value of the measured impedance; ReZ_{calc} and ImZ_{calc} are the calculated real and imaginary components respectively.

Voltammograms and capacitance versus potential curves have been measured with a 10 mV s^{-1} sweep rate, unless noted otherwise. Capacitance measurements were performed using an 18 Hz sine-wave of 10 mV peak-to-peak amplitude. All current and capacitance values are normalized with respect to the geometrical area of the electrode. The d.c. capacitance C_{dc} is calculated by dividing the current density $j(E)$ by the sweep rate dE/dt.

All measurements were performed at room temperature (20 ± 1°C). The potentials were measured and are quoted with respect to the saturated calomel electrode (SCE).

The potentials of zero charge (pzc) of the reconstructed gold surfaces in 0.1 M perchlorate solutions ($HClO_4$, $KClO_4$) were estimated from the capacitance minimum

measured for solutions of various perchlorate concentrations (5×10^{-3} M < $c(ClO_4^-)$ < 0.1 M). We obtained −0.275 and −0.280 V for Au(111)-(23 × √3) and Au(100)-(hex) respectively, which is in reasonable agreement with previously published values [12,31]. These values were used to obtain the charge density $q^M(E)$ of the Au(*hkl*) electrode in perchlorate solution from integrating $C(E)$. We have chosen $q^M(E = -0.8\,V)$ as the integration constant when calculating $q^M(E)$ curves for the neutral, bromide containing solutions from the respective voltammograms (scan rate 2 or 5 mV s^{-1}). This procedure also provided a reasonable estimate of the integration constant used for data analysis of the acidic systems. The whole strategy is based on the observation that bromide ions do not adsorb at $E \leq -0.80$ V.

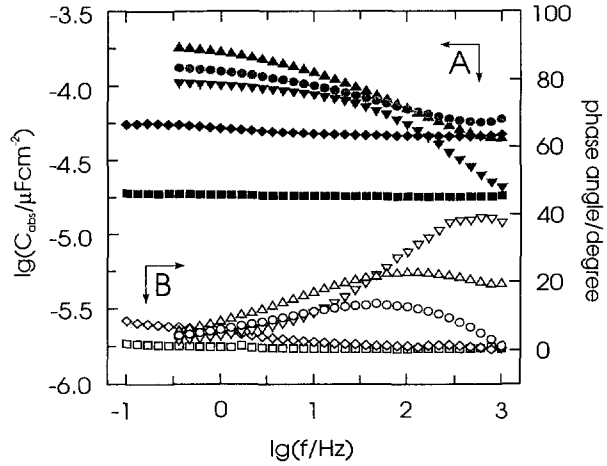

Fig. 2. Magnitude (full symbols) and phase angle (open symbols) of the complex capacitance (Bode representation) as a function of frequency for Au(111) in 0.1 M $HClO_4$ (except ■, □) under the following conditions: ■, □, 0.1 M $KClO_4$, $E = -0.60$ V; ◆, ◇, 0.1 M $HClO_4$, $E = 0.50$ V; ●, ○, 0.15 mM NaCl, $E = 0.40$ V; ▲, △, 0.15 mM NaBr, $E = 0.11$ V; ▼, ▽, 0.15 mM NaI, $E = -0.28$ V.

3. Results

3.1. Impedance behaviour of Au(111) and Au(100) in perchlorate solutions

Fig. 1 shows typical voltammograms and capacitance–potential curves for Au(111) and Au(100) in 0.1 M $KClO_4$ or 0.1 M $KClO_4$ + 1 mM $HClO_4$ solutions. We note that the perchlorate ion is only weakly specifically adsorbed at both surfaces [32]. The pH influences the limits of the accessible potential range of an ideally polarizable Au(*hkl*)|aqueous electrolyte interface. The competitive adsorption of hydroxide ions [31] modifies the cyclic voltammograms at $E > 0.20$ V, as is evident from a comparison of the neutral (solid lines in Fig. 1) and the acidic (dotted lines in Fig. 1) systems. In contrast, there is only a minor effect of the pH on the capacitance measured at 18 Hz.

Scanning the potential towards positive charge densities causes the lifting of the surface reconstruction. This process is kinetically controlled and appears rather gradually in the case of Au(111) [10]. The potential range in which the lifting of the reconstruction proceeds is somewhat narrower in the case of Au(100). The latter system also shows a significant negative shift of the pzc, which causes the pronounced maximum in the voltammogram. The re-

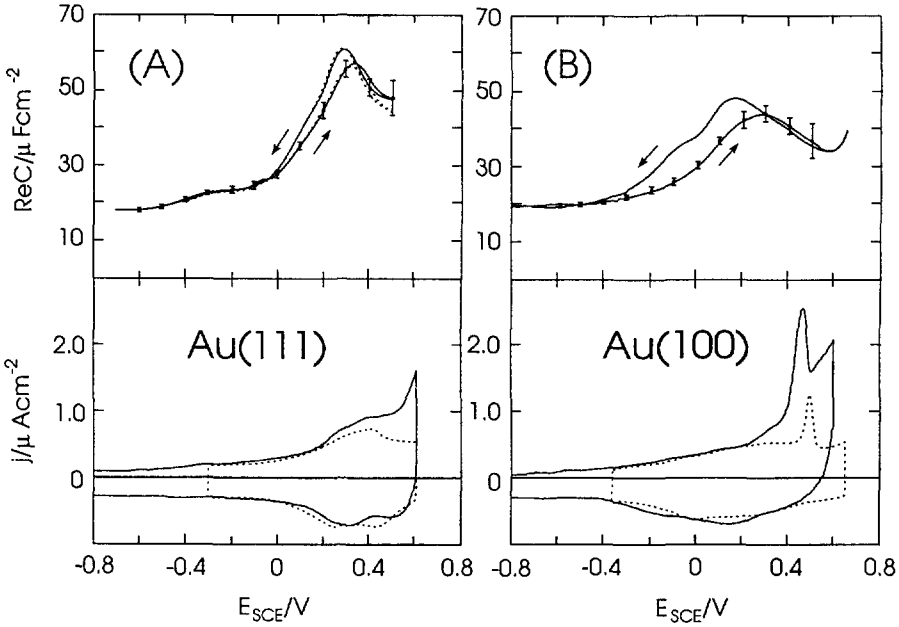

Fig. 1. Capacitance (ReC) potential curves and cyclic voltammograms for (A) Au(111) and (B) Au(100) in 1 mM $HClO_4$ + 0.1 M $KClO_4$ (dotted line) and 0.1 M $KClO_4$ (solid line). Scan rate 10 mV s^{-1}. The error bars indicate the extent of frequency dispersion of the capacitance as obtained from steady state impedance measurements with 0.1 Hz < f < 5 kHz.

formation of the reconstructed surface during the subsequent negative potential scan is rather slow for both gold faces in ClO_4^- solutions [10,21,31], and consequently adds to the hysteresis in the capacitance versus potential curves (Fig. 1). Impedance experiments revealed that the capacitance exhibits only a minor frequency dependence at potentials $E < +0.40$ V in perchlorate solutions. The ratio of the capacitances measured at 1 and 0.1 kHz differs from unity by a few per cent only. The error bars in Fig. 1(A) and Fig. 1(B) indicate the variation of the capacitance with frequency as obtained from steady state impedance measurements. At potentials $E > +0.40$ V, a definite capacitance dispersion appears, which is attributed to the adsorption of OH^- ions. This observation can be generalized. Fig. 2 illustrates that whenever anions are specifically adsorbed, a significant dispersion of the interfacial capacitance is observed. Some typical results of the Au(111)|Br^- and Au(100)|Br^- systems will be presented in the following sections.

3.2. Impedance behaviour of Au(111) in the presence of bromide ions

Fig. 3(A) shows a set of voltammograms for various bromide concentrations in 0.1 M $HClO_4$ or 0.1 M $KClO_4$. The peaks labelled P1 and P2 can be associated with the lifting of the Au(111)-(23 × √3) reconstruction [21,33] and the formation of an ordered, incommensurate hexagonal close-packed bromide adlayer [17] respectively. Whereas P2 is rather reversible, P1 exhibits no cathodic counterpart due to the slow reformation of the reconstructed Au(111)-(23 × √3) surface. In the first positive scan, the positions of P1 and P2 change by −58 mV per bromide concentration decade (cf. the inset to Fig. 3(A)). We also note that the charge due to Br^- adsorption during the positive scan is practically independent of the adsorbate (bromide) concentration for 10^{-5} M < $c(Br^-)$ < 0.05 M and amounts to approximately 90 μC cm^{-2}. The peak P1 also broadens with decreasing bromide concentration (or with increasing scan rate), which can be attributed to a more pronounced diffusion control of the anion adsorption.

The corresponding ReC and ImC vs. E curves are plotted in Fig. 3(B). Ideal capacitive behaviour was found for the Au(111)-(23 × √3) electrode in Br^- containing solutions at sufficiently negative potentials, where neither Br^- adsorbs nor hydrogen reduction proceeds. There exists a significant frequency dispersion around P1 (cf. the non-zero ImC component) and P2, which reflects the transition kinetics of the substrate surface and of the adlayer structure respectively [10,17]. In general, the extent of the capacitance dispersion depends on the bromide concentration in the potential range where bromide is specifically adsorbed on Au(111)-(1 × 1).

In order to explore the nature of the "capacitance dispersion" at potentials more positive than P1, systematic sets of "d.c. steady state" impedance spectra have been

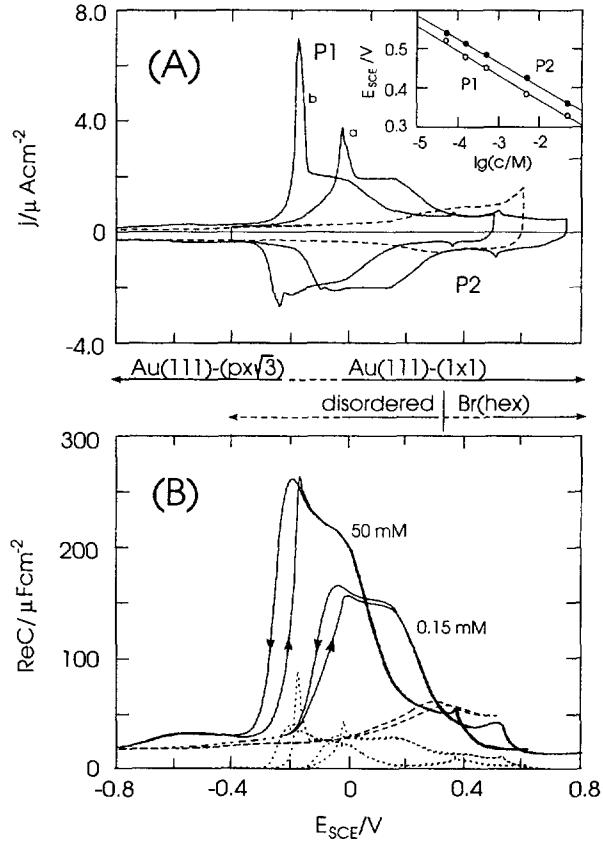

Fig. 3. (A) Cyclic voltammograms for Au(111) in 0.1 M $HClO_4$ + 0.15 mM NaBr (solid line a) and 0.05 M $KClO_4$ + 50 mM NaBr (solid line b). The voltammogram represented by the dashed line has been measured in 0.1 M $KClO_4$. The inset shows the concentration dependence of the transition peaks P1 and P2. The potential values of P1 are plotted with an offset of 0.50 V. (B) ReC (solid lines) and ImC (dotted lines) vs. potential of the same systems as in (A). Dashed line: ReC vs. potential in 0.1 M $KClO_4$. The stability ranges of the various surface (Au) and adlayer (Br) structures are also indicated. The transition regions are labelled P1 and P2.

measured in 0.1 M $HClO_4$ (or 0.1 M $KClO_4$) containing NaBr (5×10^{-5} M < $c(Br^-)$ < 5×10^{-2} M). Some typical capacitance spectra are presented in Fig. 4 for the Au(111) electrode in 0.15 mM NaBr + 0.1 M $HClO_4$, and for some other NaBr concentrations in Fig. 5. The following features are characteristic.

(1) The spectra are mostly arc-shaped, except at the limits. At the cathodic end the spectra shrink into a frequency-independent single point (cf. the spectrum at $E = -0.2$ V in Fig. 4(A)). At positive potentials past P2 the spectra can be approximated by tilted lines rather then by arcs (Fig. 4(B)).

(2) The spectra at lower potentials are of quarter circle form (cf. spectra at $E = -0.1$ and 0 V in Fig. 4(A)). Close to P2 their shape is a semicircle (cf. the spectrum at $E = 0.4$ V) and in between they resemble asymmetric arcs, the high and low frequency parts of which fit to a semicircle and quarter circle respectively. At sufficiently high and low frequencies, the capacitances can be extrapolated to

certain limiting real values, denoted by C_{HF} and C_{LF} respectively.

(3) With concentration, the shape of the arcs does not change; however, the location of the individual frequency points does change markedly. The spectra shift clockwise along the arcs with increasing concentration (Fig. 5(A)). Thus, at sufficiently low and high bromide concentrations, the spectra shrink into C_{HF} and C_{LF} respectively.

(4) Using the bromide data of Shi and Lipkowski [34] determined chronocoulometrically, we measured the impedance spectra at constant bromide surface excess by selecting appropriate potentials E and bulk concentrations

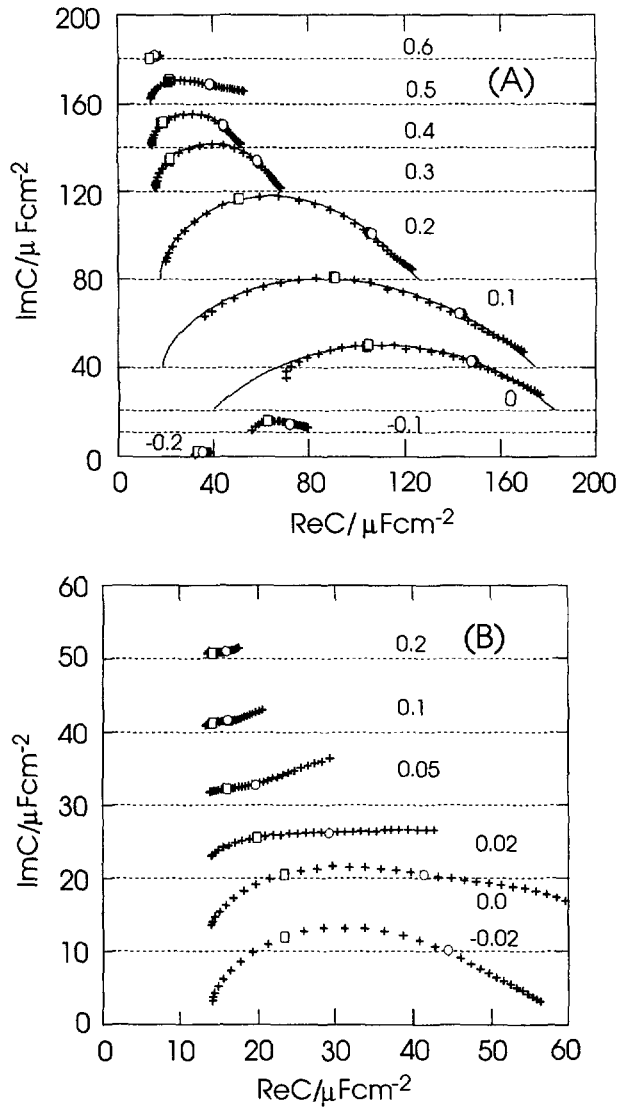

Fig. 4. (A) ImC vs. ReC representation of the steady state impedance spectra measured for Au(111) in 0.1 M $HClO_4$ + 0.15 mM NaBr at various potentials. The solid lines represent curves calculated using fitting parameters of the equivalent circuit shown in Fig. 6. The measured and calculated data at 10 Hz (○, ●) and 100 Hz (□, ■) are indicated. The spectra are shifted along the ImC direction for clarity. The dashed lines indicate the respective ImC zero lines. (B) ImC vs. ReC impedance spectra around P2 = 0.5 V. The potentials are given relative to this transition potential. The meanings of the symbols are the same as in (A).

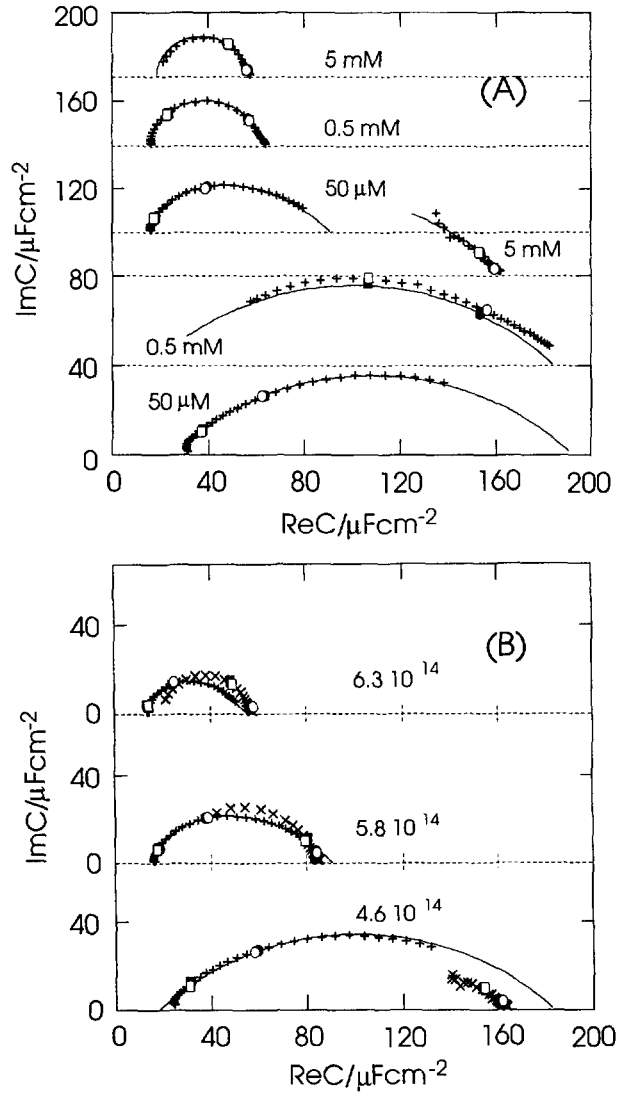

Fig. 5. ImC vs. ReC representation of the steady state impedance spectra measured for Au(111)|0.1 M $HClO_4$ in the presence of bromide ions at (A) various concentrations with $E = 0.3$ V (upper three sets) and $E = 0.1$ V (lower three sets) and (B) various bromide surface excesses (in ions cm^{-2}) as indicated. Br^- concentrations: (+) 0.05 mM; (×) 5.0 mM. The meanings of the symbols are the same as in Fig. 4.

$c(Br^-)$. The results illustrate that $C_{HF}(c(Br^-),E)_r$ and $C_{LF}(c(Br^-),E)_r$ are quite close to each other within the rather broad bromide concentration range studied (Fig. 5(B)), except for the immediate phase transition regions around P1 and P2.

The shape of the capacitance spectra and the observed concentration dependence both point to two possible major causes of the observed frequency dispersion for the Au(111)|Br^- system: (i) diffusion of the adsorbing ions to the interface, and (ii) a slow electrosorption process at the electrode surface. From an electrical point of view the slow adsorption can be modelled by an equivalent circuit containing an adsorption resistance R_{ad} and an adsorption "pseudo" capacitance C_{ad} in series. If the diffusion is also

taken into account, an additional serially connected diffusional impedance appears in the circuit. The respective impedance and capacitance functions have the following forms [26–28]:

$$Z(\omega) = R_s + \cfrac{1}{i\omega C_{dl} + \cfrac{1}{R_{ad} + \cfrac{\sigma_{ad}}{\sqrt{i\omega}} + \cfrac{1}{i\omega C_{ad}}}} \quad (1)$$

and

$$C(\omega) = \frac{1}{i\omega(Z(\omega) - R_s)} = C_{dl} + \frac{C_{ad}}{1 + \sigma_{ad} C_{ad}\sqrt{i\omega} + R_{ad} C_{ad} i\omega} \quad (2)$$

where $\sigma_{ad}(i\omega)^{-1/2}$ represents the diffusional (Warburg) impedance with its coefficient σ_{ad}. Within the framework of this model, C_{HF} and C_{LF} are identified as C_{dl}, the double layer capacitance, and $C_{dl} + C_{ad}$ respectively.

The equivalent circuit of Fig. 6, or some subset of it, along with the corresponding functions of Eq. (1) and Eq. (2), were employed to calculate the interfacial impedance of Au(111)|Br^- in the surface excess range 5×10^{13} ions $cm^{-2} < \Gamma < 65 \times 10^{13}$ ions cm^{-2} (the Γ values were taken from Ref. [34]). The parameters of Eq. (2) can be fitted satisfactorily to the measured spectra. A typical example is given in Fig. 4. The solid lines and symbols, which represent the calculated and experimental data of the complex capacitance, practically coincide. Alternatively, the whole spectrum gradually shrinks to a single capacitance value in the potential region negative of the reconstruction peak P1. The equivalent circuit simplifies there to the R_s–C_{dl} combination.

There are, however, potential regions where the impedance cannot be characterized by Eq. (1). The capacitance spectrum is either not of arc form, or the instability of the fitting procedure indicates that additional terms (circuit elements) should be taken into account. These regions are as follows: (i) at potentials more positive than that of P2, where a new process starts to dominate which yields significant capacitance dispersion (Fig. 4(B)); (ii) additional dispersion is also observed within a small potential region around P1 due to the transition kinetics.

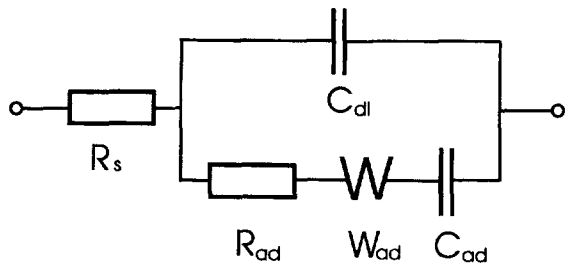

Fig. 6. Equivalent circuit of the electrode in the presence of adsorption: R_s, solution resistance; C_{dl}, double layer capacitance; C_{ad}, adsorption capacitance; R_{ad}, adsorption resistance; W_{ad}, diffusional impedance.

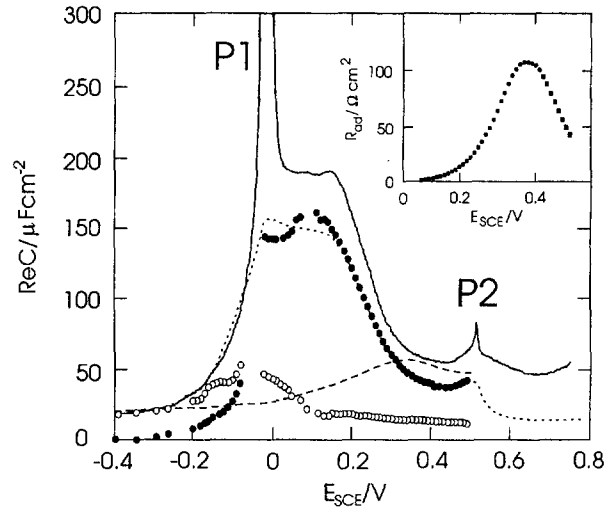

Fig. 7. C_{ad} (●) and C_{dl} (○) as a function of potential measured for Au(111) in 0.1 M $HClO_4$ containing 0.15 mM NaBr determined from impedance spectra by fitting the impedance function of the equivalent circuit of Fig. 6 to the experimental spectra. The inset shows R_{ad} as a function of potential. Note that the determination of the above parameters around the transition peak P1 was not possible. Solid line: d.c. capacitance as calculated from a cyclic voltammogram for the same system obtained at a sweep rate of 2 mV s^{-1}. Dotted line: a.c. capacitance curve measured with 1 Hz, 10 mV peak-to-peak amplitude perturbation, with 2 mV s^{-1} sweep rate. Dashed line: a.c. capacitance (18 Hz) measured in 0.1 M $KClO_4$.

A typical potential dependence of the fitted parameters C_{dl}, C_{ad} and R_{ad} is shown in Fig. 7. We included the d.c. capacitance curve of the same system calculated from the positive branch of the corresponding cyclic voltammogram (scan rate 2 mV s^{-1}) by $C_{dc} = j(E)/(dE/dt)$. This "zero-frequency, zero-amplitude" capacitance curve serves as an "envelope-curve", i.e. it should be, and in fact is, the sum of C_{dl} and C_{ad} everywhere except for the phase transition regions. For comparison, we have also plotted the anodic branch of the a.c. capacitance measured at 1 Hz with 10 mV peak-to-peak amplitude (dotted line in Fig. 7). The latter is much less than $C_{LF} = C_{dl} + C_{ad}$ and, as such, is not suitable for extracting thermodynamic data.

3.3. Impedance behaviour of Au(100) in the presence of bromide ions

Fig. 8 shows voltammograms and complex capacitance curves measured for Au(100) in 0.1 M $HClO_4$ + 0.15 mM Br^- and in 50 mM $KClO_4$ + 50 mM Br^- solutions. P1 corresponds to the lifting of the Au(100)-(hex) reconstruction [21,31], while P2 and P3 represent two phase transitions within the bromide adlayer (P2, disorder ⇌ c($\sqrt{2} \times 2\sqrt{2}$); P3, c($\sqrt{2} \times 2\sqrt{2}$) ⇌ c($\sqrt{2} \times$ p)) [35]. The stability ranges of the respective substrate surface and adlayer structures are indicated.

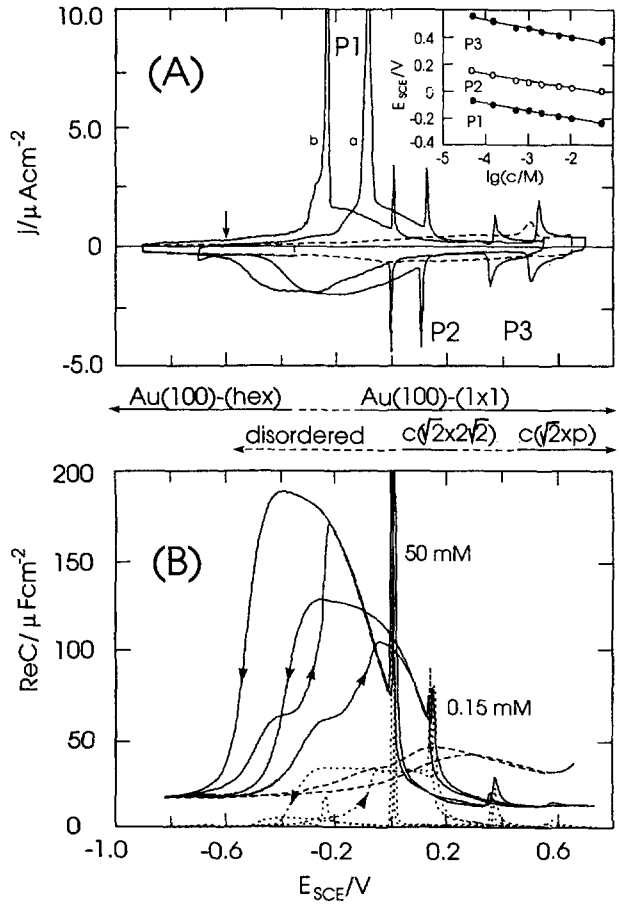

Fig. 8. (A) Cyclic voltammograms for Au(100) in 0.1 M $HClO_4$ containing 0.15 mM NaBr (solid line a) and 0.05 M $KClO_4$ containing 50 mM NaBr (solid line b). The dashed line represents the voltammogram in 0.1 M $KClO_4$. The inset shows the concentration dependence of the transition peaks P1, P2 and P3. The potential values of P2 and P3 are the average of the first positive and negative scans. (B) ReC (solid lines) and ImC (dotted lines) vs. potential of the same systems as in (A). Dashed line: ReC vs. potential in 0.1 M $KClO_4$. All curves represent first scans obtained just after immersion of the gold electrode at negative potentials. The structures of the surface (Au) and adlayer (Br) are also indicated. The transition regions are labelled P1, P2 and P3.

The impedance spectra for the region negative to P3 are, in general, of arc shape. They can be fitted by the equivalent circuit of Fig. 6. The potential dependence of the fitted parameters for the 0.15 mM Br^-|0.1 M ClO_4^- system is presented in Fig. 9. We also plotted the a.c. capacitance measured with $f = 1$ Hz (dotted line) and the d.c. capacitance obtained from a corresponding slow-scan voltammogram (solid line, 2 mV s^{-1}).

Complications exist in the transition regions close to P1, P2 and P3. Around P2, for example, there is a sharp peak in the C_{LF} vs. E (or C_{dc} vs. E) and therefore also in the C_{ad} vs. E plot, while the shape of C_{HF} vs. E is practically uninfluenced. Typical capacitance spectra measured at potentials in the vicinity of P2 are shown in Fig. 10. Since this phase transition proceeds in a very narrow potential range, the strong non-linearity of C_{ad} leads to an

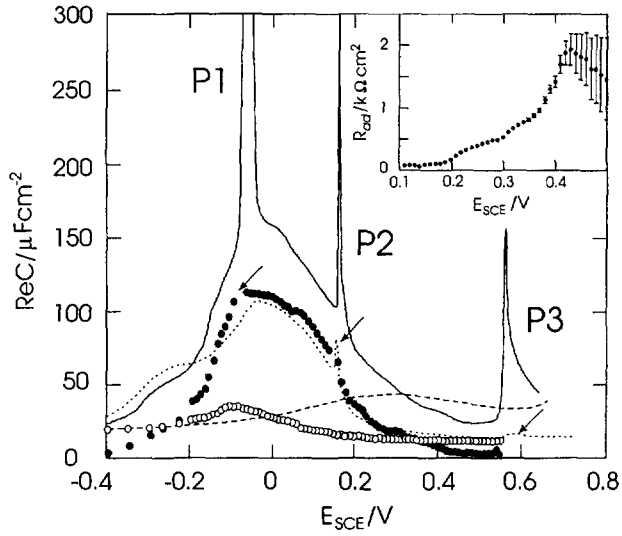

Fig. 9. C_{ad} (●) and C_{dl} (○) as a function of potential for Au(100) in 0.1 M HCO_4 + 0.15 mM NaBr determined from impedance spectra by fitting the impedance function of the equivalent circuit of Fig. 6 to the experimental data. The inset shows R_{ad} as a function of potential. Error bars indicate the precision of the calculated parameters. Solid line: d.c. capacitance calculated from the corresponding cyclic voltammogram at a sweep rate of 2 mV s^{-1}. Dotted line: a.c. capacitance curve measured with 1 Hz, 10 mV peak-to-peak amplitude perturbation, with 2 mV s^{-1} sweep rate. Dashed line: a.c. capacitance (18 Hz) measured in 0.1 M $KClO_4$.

amplitude dependence of the impedance, even at a.c. amplitudes as low as 0.4 mV. Despite this fact we notice that the (ReC,ImC) data points at potentials just on top of P2 seem to scale equidistantly with the decadic logarithm of the a.c. frequency for $\omega \rightarrow 0$. Furthermore, we found that neither the shape of the capacitance spectra, nor the value

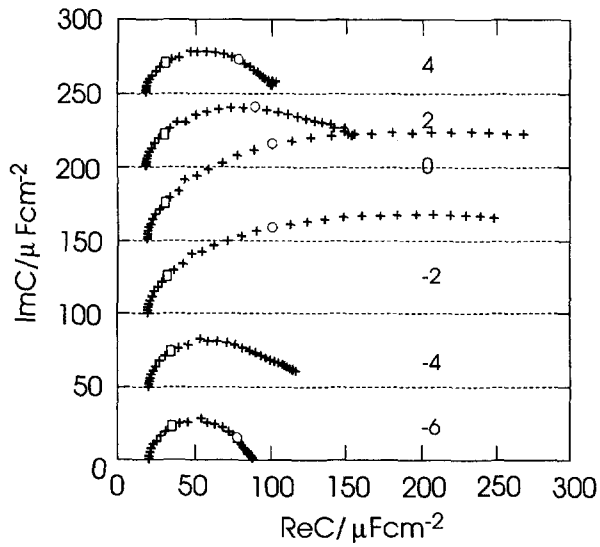

Fig. 10. ImC vs. ReC representation of the impedance spectra for Au(100) in 0.1 M $HClO_4$ + 0.15 mM NaBr at various potentials around P2. The potentials (mV) are given relative to the transition potential E(P2) = 0.124 V.

of the fitted parameters on both sides of the phase transition, change substantially with a.c. amplitude.

The impedance/capacitance behaviour of the Au(100) electrode in the presence of Br^- at potentials positive of P3 is similar to that of the Au(111)|Br^- system beyond P2, i.e. the capacitance spectra are tilted lines.

4. Discussion

4.1. Equilibrium quantities

4.1.1. General

Most of our experiments with gold single crystal electrodes have been carried out during the first positive scan with a freshly flame-annealed crystal. Thus the measurements at potentials negative of P1 have been made on electrodes with a reconstructed surface. Experiments at potentials past the lifting of the reconstruction were performed on gold electrodes with a thermodynamically stable (1×1) surface structure. The slow kinetics of the reformation of the reconstructed surface, after having been lifted, during the subsequent negative scan did not allow us to measure steady state impedance spectra for Au(*hkl*)-(1×1) at potentials negative of P1.

We would like to stress that our single crystal electrodes Au(111) and Au(100) did not show any significant frequency dispersion of the interfacial capacitance in the absence of specifically adsorbed anions. No effects due to surface heterogeneity, as are known for the case of ideally polarizable microscopically rough and irregular electrodes [20], were found.

The capacitance dispersion observed in our experiments can be traced back to two major sources.

(1) *Phase transitions at the interphase.* This can be the lifting of the reconstruction, the reformation of the reconstructed surface or phase transitions within the adlayer.

(2) *Specific adsorption of anions.* The frequency dispersion of the capacitance can be attributed to the slowness of the adsorption (electrosorption) step and/or of the diffusion of the adsorbing species. Capacitance dispersion of this type can be adequately described by the classical adsorption impedance theories.

The thermodynamic parameters, which characterize the equilibrium state of the electrode, can be derived from two capacitances: $C_{dl} = (\partial q^M/\partial E)_\Gamma$ and $C_{ad} = (dq/dE) - (\partial q/\partial E)_\Gamma$. These quantities, irrespective of the impedance model of the interface, can be identified as C_{HF} and $C_{LF} - C_{HF}$.

We have shown in Fig. 5(B) that the spectra shrink, at constant surface excess of the adsorbate, towards the C_{HF} (C_{LF}) points with decreasing (increasing) concentration of the specifically adsorbed bromide ions. A practical consequence of this behaviour is that C_{HF} (C_{LF}) can be measured accurately in solutions of low (high) adsorbate concentrations, within the easily accessible frequency range of 0.1 Hz to 5 kHz. However, one cannot extrapolate to the C_{LF} points in the vicinity of the phase transitions even in high concentration solutions (cf. Fig. 5(B) and Fig. (10)). Further elements have to be added to the equivalent circuit given in Fig. 6 (cf. the discussion in Ref. [36]).

There is an alternative way of obtaining the (almost) equilibrium values of C_{LF} in the absence of a faradaic reaction. One can calculate the d.c. capacitance C_{dc} from the slow-scan ($dE/dt < 5\,mV\,s^{-1}$) voltammograms by

$$C_{dc}(E) = j(E)/(dE/dt) = dq/dE \quad (3)$$

Provided the scan rate is sufficiently small and the inherent time-dependence of q can be neglected (e.g. q approaches its steady state value), C_{dc} can be understood as the "zero-frequency, zero-amplitude" limit of the interfacial capacitance under equilibrium conditions, C_{LF}. For the case of an adsorption-controlled process C_{LF} represents the sum of the double layer and adsorption capacitances $(C_{dl} + C_{ad})$.

As an example, the data of Fig. 7 and Fig. 9 illustrate that $C_{dl} + C_{ad}$, the sum of the capacities represented by the full and open circles, approaches C_{dc} (shown as a solid line) at constant potential everywhere except around the phase transition regions. Impedance measurements in the latter regions are difficult to perform and subsequently to interpret, since either the surface is not in the steady state or the electrical parameters are highly non-linear (as around P2 of the Au(100)|Br^- system). Fig. 7 and Fig. 9 also demonstrate that the a.c. capacitance C_{ac}, as obtained in a potential scan experiment at one frequency (even as low as 1 Hz), cannot be considered to be a truly equilibrium quantity and, as such, caution has to be exercised in any thermodynamic analysis using this data. $C_{LF} = C_{dl} + C_{ad}$ as well as C_{dc} are significantly larger than C_{ac}.

All capacitances discussed above contain contributions from the diffuse layer. The separation of the Helmholtz capacitance C_H from the diffuse layer capacitance C_d is based on the premise that the experimentally accessible equilibrium capacitance C (both of C_{dl} and C_{LF}) in the presence of specifically adsorbed ions can be expressed by the following equation [37]:

$$\frac{1}{C} = \frac{1}{C_H} + \left(1 - F\frac{\partial \Gamma}{\partial q^M}\right)\frac{1}{C_d} \quad (4)$$

Recent theories suggest that C_H contains contributions from both the solution and the metal at the interface [38]. Firstly, the solution shows considerable structure at the interface due to the finite size of the ions and solvent molecules and their field-dependent orientation behaviour, which may change the dielectric constant of the interfacial region. Secondly, the surface potential χ of the metal varies with the applied surface charge, thus modifying the potential distribution across the interface.

4.1.2. Interfacial capacitance

Steady state impedance experiments revealed that the weakly adsorbed ClO_4^- ion causes only a minor frequency

dispersion of the interfacial capacitance of Au(111) and Au(100) electrodes, e.g. $C_{dc} \approx C_{LF} \approx C_{HF} \approx C_{dl}$. For comparison, C_{dl}, which corresponds to the interfacial capacitance in "frozen" adsorption equilibrium ($\omega \rightarrow \infty$), is plotted as a function of the total formal charge of the gold electrodes q^M in Fig. 11 (solid lines). Both curves have a well-defined maximum, which in the case of the Au(111)-$(23 \times \sqrt{3})$|0.1 M $KClO_4$ system is slightly shifted towards positive charge densities. For comparison, Fig. 11 also contains the frequency-independent Helmholtz capacity C_H values of other selected systems: Au(100)|1.0 M $HClO_4$ [32] and Ag(100)|0.02 M NH_4ClO_4 [39]. The shapes of all four curves indicate the decrease of the capacitance with increasing absolute value of the applied electric field. This has been attributed to the dielectric saturation which lowers the interfacial dielectric constant and thus the capacitance [40]. The data also illustrate that the experimental C_{dl} vs. E curves of Au(100)-(hex) or Au(111)-$(23 \times \sqrt{3})$|0.1 M ClO_4^- still contain a non-negligible contribution of the diffuse layer capacitance C_d, especially around $q^M = 0$. Unfortunately, the latter could not be determined satisfactorily using the Gouy–Chapman approach [32]. This situation is somewhat less complicated for the specifically adsorbed halide ions on both gold surfaces, where the diffuse layer contribution to the experimentally measured capacitance curves can be neglected, provided that the overall ionic strength is sufficiently high. Shi and Lipkowski [41] showed that, for the specific adsorption of chloride on Au(111) (ionic strength 0.1 M), the experimentally accessible equilibrium capacitance C practically represents the Helmholtz capacitance C_H. Similar results were reported by Valette et al. [37] for halide ions adsorbed on Ag(*hkl*). We found that C_{dl}, which can now be understood as the high frequency limit of the Helmholtz capacitance,

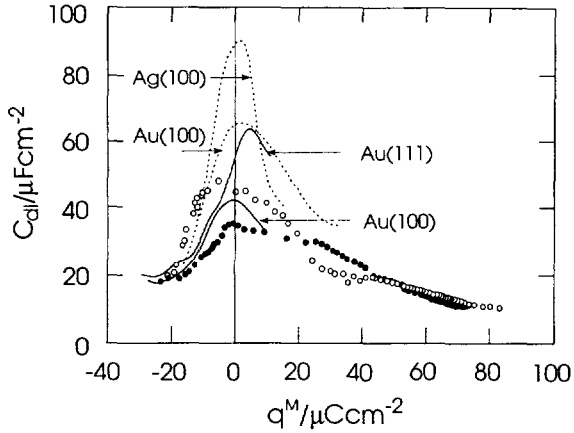

Fig. 11. Double layer capacitance C_{dl} as a function of the formal electrode charge density for the systems Au(100)|0.15 mM NaBr|0.1 M $HClO_4$ (●); Au(111)|0.15 mM NaBr|0.1 M $HClO_4$ (○); Au(111) or Au(100)|0.1 M $HClO_4$ (—). The Helmholtz capacities of Ag(100)|0.02 M NH_4ClO_4 [39] and Au(100)|1.0 $HClO_4$ [32] are also shown (dotted lines).

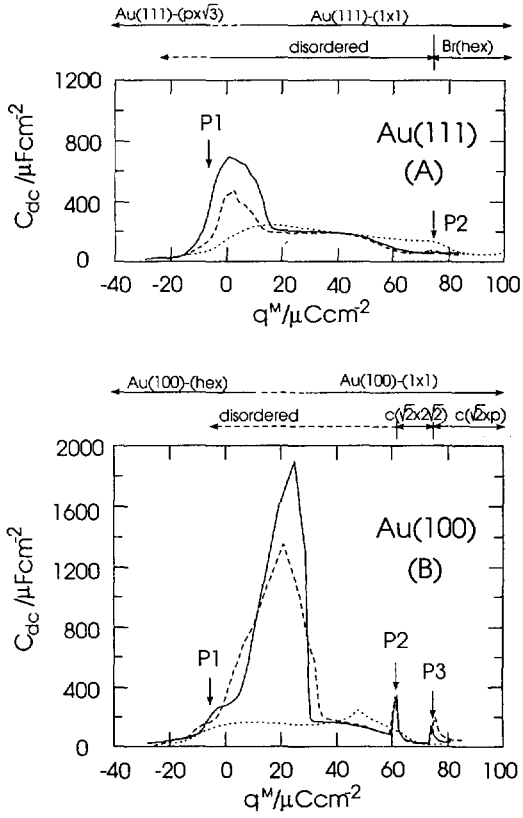

Fig. 12. D.c. capacitance C_{dc} as a function of the formal electrode charge density q^M: (A) Au(111) and (B) Au(100) in 0.1 M $KClO_4$ + 0.15 mM NaBr (dashed line) and 50 mM $KClO_4$ + 50 mM NaBr (solid line). For comparison, the $C_{dc} - q^M$ curves of the following systems have been added: 50 mM NaBr|50 mM $KClO_4$|Ag(111), dotted line in (A); 50 mM NaBr|50 mM $KClO_4$|Ag(100), dotted line in (B).

is only weakly dependent on the bromide concentration for $|q^M| > 10\ \mu C\ cm^{-2}$ and 0.1 M $ClO_4^-|x$ M NaBr with $x < 10^{-3}$. The corresponding capacitance of the systems containing non-specifically adsorbed ions is approached at higher negative and positive fields. In contrast, C_{dl} around the pzc is significantly lower in the presence of bromide ions than that of systems containing only weakly specifically adsorbed ions like ClO_4^- or PF_6^- [42]. Such an observation has been interpreted as a widening of the Helmholtz region, which is either caused by: (i) the direct presence of bromide ions, as is also discussed for the $Br^-|Hg$ system [43]; or (ii) indirectly by substrate changes due to the bromide ion induced surface stress [44]. Neither of the effects are clearly understood at present.

Our impedance measurements also showed that the low frequency capacitance C_{LF} of the bromide|Au(*hkl*) systems can be described fairly well by the sum of C_{dl} and C_{ad}, except for the phase transition regions (Fig. 7 and Fig. 9). However, C_{dc} approaches the equilibrium interfacial capacitance over the entire potential region investigated when measured at sufficiently low sweep rates. The latter is plotted in Fig. 12 as function of surface charge q^M for

the cases of bromide adsorbed on the (111) and (100) faces of gold (solid and dashed lines) and on silver single crystals (dotted curves) [45] for comparable concentrations and ionic strengths. Obviously, for both gold systems the positions of the substrate and adlayer transitions P1 and P2 (Au(111)) or P1, P2 and P3 (Au(100)) are practically independent of the bromide concentrations. The onset of the lifting of the Au(111)-(23 × √3) reconstruction takes place at $-10 \pm 2\,\mu C\,cm^{-2}$, and the entire process consumes up to $25\,\mu C\,cm^{-2}$. The structural changes of the Au(100)-(hex) phase seem to proceed in two steps. A well-developed shoulder precedes the main peak P1. The shoulder occurs around $-10 \pm 5\,\mu C\,cm^{-2}$ in $10^{-4}\,M < c(Br^-) < 0.1\,M$ and is most probably related to the onset of the lifting of the Au(100)-(hex) reconstruction, which occurs mainly in P1. The main peak P1 is shifted towards positive charge densities (around $20\,\mu C\,cm^{-2}$) compared with Au(111) (around $0\,\mu C\,cm^{-2}$). Alternatively, the capacitive contribution due to the reconstruction of the gold surface structure adds practically on top of a broad peak. This broad peak is rather similar for gold and silver surfaces, as shown in Fig. 12, and rather independent of the crystal orientation. This feature has been associated with the adsorption of solvent molecules and randomly adsorbed bromide ions, reflecting both similar screening properties of the two metals and similar surface dipole moments in the presence of bromide [41,46].

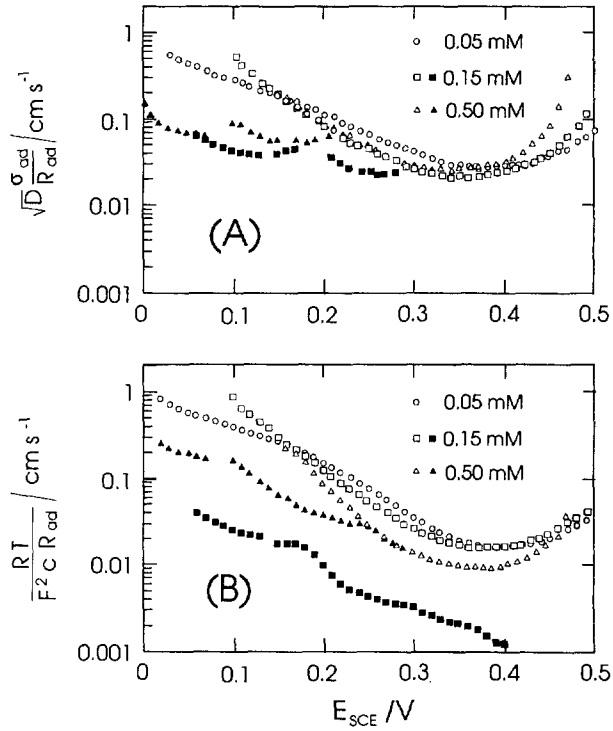

Fig. 13. Rate parameter (A) $\partial\nu/\partial c = \sqrt{D}\sigma_{ad}/R_{ad}$ and (B) $RT/(F^2 c(Br^-)R_{ad})$ calculated for the systems with mixed diffusion- and rate-controlled adsorption. The open and filled symbols represent the unreconstructed phases of Au(111)-(1 × 1) and Au(100)-(1 × 1) respectively. The base electrolyte was always 0.1 M $HClO_4$. The error bars are within the size of the symbols.

4.2. Kinetic aspects

As has been shown in Section 3.2, the equivalent circuit of Fig. 6 is adequate for the analysis of our impedance spectra in a fairly broad potential range and in a certain range of adsorbate (Br^-) concentrations.

Following the usual derivation scheme of the adsorption impedance, we assume an overall one-step electrosorption reaction. The net-rate of adsorption, $\nu(t)$, is expressed in general terms as

$$\nu(t) = \frac{d\Gamma}{dt} = \nu(E, c_s, \Gamma) = \nu_{ad}(E, c_s, \Gamma) - \nu_{des}(E, \Gamma) \tag{5}$$

with

$$\nu_{ad} = k_{ad} c_s f_{ad}(\Gamma) \text{ and } \nu_{des} = k_{des} f_{des}(\Gamma) \tag{6}$$

where c_s is the surface concentration of the adsorbing species, k_{ad} and k_{des} are the adsorption and desorption rate coefficients. $f_{ad}(\Gamma)$ and $f_{des}(\Gamma)$ are monotonically decreasing and increasing functions of the surface excess Γ respectively. We normalize the f functions by regarding the limiting cases to be $f_{ad}(\Gamma \to 0) = 1$; $f_{ad}(\Gamma \to \Gamma_{max}) = 0$; $f_{des}(\Gamma \to 0) = 0$; $f_{des}(\Gamma \to \Gamma_{max}) = 1$.

Assuming semi-infinite planar diffusion of the adsorbing species, analogously to the derivations of Frumkin and Melik-Gaykazyan [26], Berzins and Delahay [27] and Lorenz and Möckel [18], one can obtain the following relations between the experimentally defined adsorption parameters C_{ad}, R_{ad}, σ_{ad} and the partial derivatives of the net adsorption rate $\nu(E, c_s, \Gamma)$:

$$\frac{\partial\nu}{\partial c_s} = \sqrt{D}\frac{\sigma_{ad}}{R_{ad}} = k_{ad} f_{ad}(\Gamma) \tag{7}$$

$$\frac{\partial\nu}{\partial\Gamma} = \frac{-1}{C_{ad} R_{ad}} = k_{ad} c_s \frac{df_{ad}(\Gamma)}{d\Gamma} - k_{des}\frac{df_{des}(\Gamma)}{d\Gamma} \tag{8}$$

$$\frac{\partial\nu}{\partial E} = \frac{-1}{\gamma F R_{ad}} = \frac{dk_{ad}}{dE} c_s f_{ad}(\Gamma) - \frac{dk_{des}}{dE} f_{des}(\Gamma) \tag{9}$$

where $\gamma = -(1/F)(dq^M/d\Gamma)_E$ is the electrosorption valency [47].

The right-hand side of Eq. (7) can also be obtained from Eq. (9) assuming equilibrium conditions and a Butler–Volmer analogue exponential potential dependence of the rate coefficients:

$$k_{ad} f_{ad}(\Gamma) = \frac{RT}{n\gamma^2 F^2 c R_{ad}} \tag{10}$$

The parameter combination of the right-hand side of Eq. (7) and Eq. (10) yields similar results and is plotted in Fig. 13 as a function of the potential for various concentrations

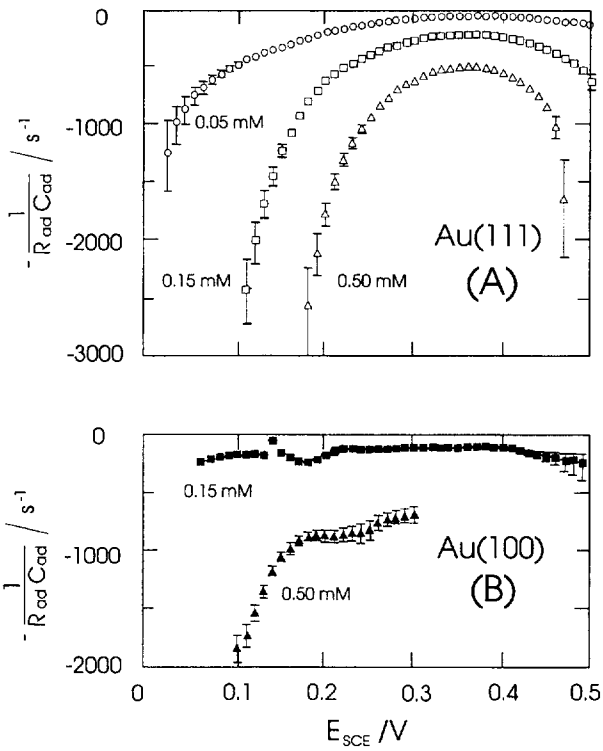

Fig. 14. Rate parameter $\partial\nu/\partial\Gamma = -1/(C_{ad}R_{ad})$ for various bromide concentrations in 0.1 M $HClO_4$ and (A) Au(111), (B) Au(100) electrodes.

of bromide on Au(111) and Au(100) respectively. This quantity:

– is smaller on Au(100) than on Au(111) by about one order of magnitude;

– monotonically decreases with potential at constant concentration in the potential region where bromide forms a disordered adlayer. This trend levels off when approaching the disorder/order transitions of the bromide adlayer around P2, owing to the fact that the adsorption impedance model of Eq. (10) is not adequate around and beyond P2 (cf. the semicircle spectra negative to and the tilted line shape spectra positive to the P2 potential in Fig. 7). The finding that $k_{ad}f_{ad}(\Gamma)$ decreases with potential indicates that the decrease of $f_{ad}(\Gamma)$ overcompensates for the increase of k_{ad} with potential.

The rate parameter $\partial\nu/\partial\Gamma$ was obtained from C_{ad} and R_{ad} (Fig. 14). The data are markedly dependent on the potential and the bromide concentration within the potential region of the disordered adlayer. The potential dependence levels off for Au(100) with the formation of the $c(\sqrt{2}\times 2\sqrt{2})$ phase. The concentration dependence goes along with a decrease in time constant of the reaction-controlled process with bromide concentration.

5. Conclusions

(1) Au(111) and Au(100) electrodes do not show any significant frequency dispersion of the interfacial capacitance ($0.1\,\text{kHz} \le f \le 5\,\text{kHz}$) in the absence of specifically absorbed anions. No effects due to surface heterogeneity, as are well known for the case of ideally polarizable rough and irregular electrodes [20], were found.

(2) The capacitance dispersion observed on Au(111) and Au(100) can be traced back to the following factors.

Phase transitions at the interphase. This can be the lifting of the reconstruction, the reformation of the reconstructed surface or phase transitions within the adlayer. These processes are often slow. Therefore, special precautions and appropriate test experiments have to be taken into account in order to define the conditions for truly "steady state" impedance measurements.

Specific adsorption of anions. The frequency dispersion of the capacitance can be attributed to the slowness of the adsorption (electrosorption) step and/or the diffusion of the surface active species. Capacitance dispersions of this type can be adequately described by the classical adsorption impedance theories.

Obviously, both factors may combine in certain potential regions.

(3) Thermodynamic and kinetic parameters can be determined from impedance measurements, providing the possibility of appropriate extrapolations of the capacities to infinite and zero frequencies. Another way of extrapolating to zero frequency is to calculate the d.c. capacitance from slow-scan voltammograms.

If the measured impedances comply with the adsorption impedance model expressed by the circuit of Fig. 6 and/or the corresponding Eq. (1) and Eq. (2), then the actual adsorption rate coefficient $k_{ad}f_{ad}(\Gamma)$ can be determined from the spectra by the methods summarized in Section 4. For the adsorption of Br on gold surfaces, $k_{ad}f_{ad}(\Gamma)$ was found to be of the order of 10^{-3} to $1\,\text{cm}\,\text{s}^{-1}$.

Acknowledgements

T.P. acknowledges a fellowship from the Alexander von Humboldt Foundation. T.W. acknowledges the support of the Deutsche Forschungsgmeinschaft through a Heisenberg fellowship. The authors are indebted to Professor R. de Levie and Professor W. Schmickler for their helpful comments.

References

[1] J. Lipkowski and L. Stolberg, in J. Lipkowski and P.N. Ross (Eds.), Adsorption of Molecules at Metal Electrodes, VCH, New York, 1992, p. 171.

[2] M.F. Toney and O.M. Melroy, in H.D. Abruna (Ed.), Electrochemical Interfaces, VCH, New York, 1991, p. 57.

[3] A. Hamelin, T. Vitanov, E. Sevastyanov and A. Popov, J. Electroanal. Chem., 145 (1983) 225.

[4] A. Hamelin, in B.E. Conway, R.E. White and J.O.M. Bockris (Eds.), Modern Aspects of Electrochemistry, Vol. 16, Plenum Press, New York, 1987, p. 1.

[5] D.M. Kolb, in R.J. Gale (Ed.), Spectroelectrochemistry – Theory and Applications, Plenum Press, New York, 1988, p. 87.
[6] P.A. Christensen and A. Hamnett, in R.G. Compton and A. Hamnett (Eds.), Comprehensive Chemical Kinetics, Vol. 29, Elsevier, Amsterdam, 1989, p. 1.
[7] G.L. Richmond, in H. Gerischer and C.W. Tobias (Eds.), Advances in Electrochemical Science and Engineering, Vol. 2, VCH, New York, 1992, p. 142.
[8] S. Manne, P.K. Hansma, J. Massie, V.B. Elings and A.A. Gewirth, Science, 251 (1991) 183.
[9] A.A. Gewirth and H. Siegenthaler (Eds.), Nanoscale Probes of the Solid/Liquid Interface, Kluwer Academic, Dordrecht, 1995.
[10] J. Wang, B. Ocko, A.J. Davenport and H.I. Isaacs, Phys. Rev. B, 46 (1992) 10321.
[11] M.F. Toney, J.N. Howard, J. Richer, G.L. Borges, J.G. Gordon, O.R. Melroy, D.G. Wiesler, D. Yee and L.B. Sorensen, Nature, 368 (1994) 444.
[12] D.M. Kolb, in J. Lipkowski and P.N. Ross (Eds.), Structure of Electrified Interfaces, VCH, New York, 1993, p. 65.
[13] N. Batina, T. Will and D.M. Kolb, Discuss. Faraday Soc., 94 (1992) 93.
[14] G. Staikov, K. Jüttner, W.J. Lorenz and E. Budevski, Electrochim. Acta, 39 (1994) 1019.
[15] O.M. Magnussen, J. Hageböck, J. Holos and R.J. Behm, Faraday Discuss., 94 (1992) 329.
[16] X. Gao, G.J. Edens, F.C. Liu, A. Hamelin and M.J. Weaver, J. Phys. Chem., 98 (1994) 8086.
[17] O.M. Magnussen, B.M. Ocko, R.R. Adzic and J. Wang, Phys. Rev. B, 51 (1995) 5510.
[18] W. Lorenz and F. Möckel, Z. Elektrochem., 60 (1956) 507.
[19] R.D. Armstrong, W.P. Rice and H.R. Thirsk, J. Electroanal. Chem., 16 (1968) 517.
[20] T. Pajkossy, J. Electroanal. Chem., 364 (1994) 111.
[21] A. Hamelin, J. Electroanal. Chem., 142 (1982) 299.
[22] C.N. van Huong, C. Hinnen, J.P. Dalbera and R. Parsons, J. Electroanal. Chem., 125 (1981) 177.
[23] J. Lipkowski, C.N. van Huong, C. Hinnen, R. Parsons and J. Chevalet, J. Electroanal. Chem., 143 (1983) 375.
[24] V.D. Jovic, B.M. Jovic and R. Parsons, J. Electroanal. Chem., 290 (1990) 257.
[25] V.D. Jovic, R. Parsons and B.M. Jovic, J. Electroanal. Chem., 339 (1992) 327.
[26] A.N. Frumkin and V.I. Melik-Gaykasyan, Dokl. Akad. Nauk., 5 (1951) 855.
[27] T. Berzins and P. Delahay, J. Phys. Chem., 59 (1955) 906.
[28] W. Lorenz, Z. Phys. Chem. NF, 26 (1958) 192.
[29] R. Oeglehaus, J. Rose and H. Baltruschat, J. Electroanal. Chem., 376 (1994) 127.
[30] N. Batina, A.S. Dakkouri and D.M. Kolb, J. Electroanal. Chem., 370 (1994) 87.
[31] D.M. Kolb and J. Schneider, Electrochim. Acta, 31 (1986) 929.
[32] F. Silva, M.J. Sottomayor, A. Hamelin and L. Stoicoviciu, J. Electroanal. Chem., 295 (1990) 301.
[33] B.M. Ocko, O.M. Magnussen, R.R. Adzic, J.X. Wang, Z. Shi and J. Lipkowski, J. Electroanal. Chem., 376 (1994) 35.
[34] Z. Shi and J. Lipkowski, J. Electroanal. Chem., 369 (1994) 283.
[35] Th. Wandlowski, J. Wang, B.M. Ocko and O.M. Magnussen, J. Phys. Chem., 100 (1996) 10277.
[36] Th. Wandlowski and R. de Levie, J. Electroanal. Chem., 352 (1993) 279.
[37] G. Valette, A. Hamelin and R. Parsons, Z. Phys. Chem. NF, 113 (1978) 71.
[38] W. Schmickler, in J. Lipkowski and P.N. Ross (Eds.), Structure of Electrified Interfaces, VCH, New York, 1993, p. 201.
[39] G. Valette, J. Electroanal. Chem., 138 (1982) 37.
[40] R. Parsons, J. Electroanal. Chem., 59 (1975) 229.
[41] Z. Shi and J. Lipkowski, J. Electroanal. Chem., 403 (1996) 225.
[42] A. Hamelin and L. Stoicoviciu, J. Electroanal. Chem., 234 (1987) 43.
[43] W. Lorenz, Z. Phys. Chem., 224 (1963) 145.
[44] G. Láng and K.E. Heusler, J. Electroanal. Chem., 391 (1995) 169.
[45] Th. Wandlowski, unpublished data.
[46] W. Schmickler and R. Guidelli, J. Electroanal. Chem., 235 (1987) 387.
[47] J.W. Schultze and F.D. Koppitz, Electrochim. Acta, 21 (1976) 327.